Potential energy landscape of a coarse grained model for water: ML-BOP

Special Collection: Water: Molecular Origins of its Anomalies

Andreas Neophytou; Francesco Sciortino ✉ (iD)
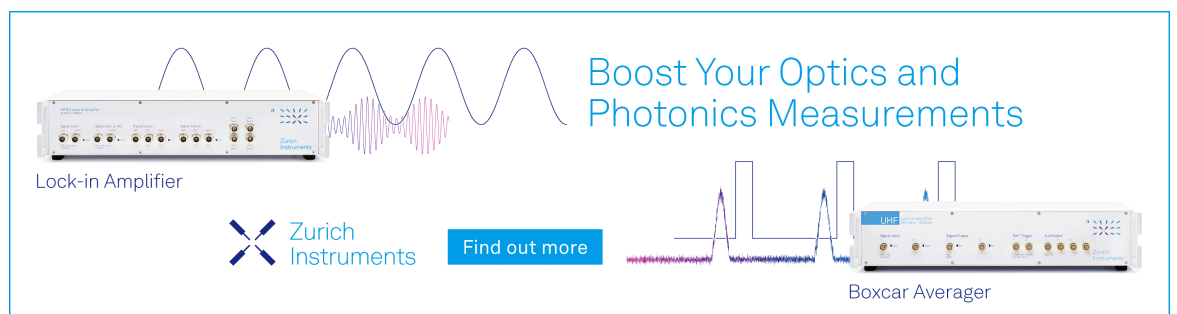
Check for updates

CrossMark

View Online

Export Citation

18 March 2024 09:23:37

Potential energy landscape of a coarse grained model for water: ML-BOP

View Online   Export Citation   CrossMark

Andreas Neophytou and Francesco Sciortino[a] (iD)

AFFILIATIONS

Department of Physics Sapienza–University of Rome, Piazzale Aldo Moro 5, I-00185 Roma, Italy

Note: This paper is part of the JCP Special Topic on Water: Molecular Origins of its Anomalies.
[a] Author to whom correspondence should be addressed: francesco.sciortino@uniroma1.it

ABSTRACT

We quantify the statistical properties of the potential energy landscape for a recently proposed machine learning coarse grained model for water, machine learning-bond-order potential [Chan *et al.*, Nat. Commun. 10, 379 (2019)]. We find that the landscape can be accurately modeled as a Gaussian landscape at all densities. The resulting landscape-based free-energy expression accurately describes the model properties in a very wide range of temperatures and densities. The density dependence of the Gaussian landscape parameters [total number of inherent structures (ISs), characteristic IS energy scale, and variance of the IS energy distribution] predicts the presence of a liquid–liquid transition located close to $P = 1750 \pm 100$ bars and $T = 181.5 \pm 1$ K.

Published under an exclusive license by AIP Publishing. https://doi.org/10.1063/5.0197613

I. INTRODUCTION

Machine learning approaches are providing more and more accurate interaction potentials for many-body systems by either (i) improving the parameters of pre-existing functional forms[1] or (ii) providing new numerical representations built from high quality quantum mechanical calculations.[2–4] Recently, approach (i) has been applied to water to produce a computationally efficient atomistic model [named machine learning-bond-order potential (ML-BOP)] that accurately reproduces the structural properties and thermodynamic anomalies of both water and ice at mesoscopic scales.[1] Similar to the mW model,[5,6] the ML-BOP model describes a water molecule as a single interacting site, accounting for the directional interactions (the hydrogen bonds in real water) via a many-body interaction contribution. The ML-BOP model[1] correctly estimates the temperature of the maximum density ice–liquid coexistence curve. As a result, this model is receiving significant attention from the water community.[7–11]

Starting from Goldstein's studies,[12] liquid properties (both dynamic and thermodynamic) have been computed by extracting information from the potential energy landscape (PEL): the multidimensional surface describing the potential energy for a system as a function of all molecular coordinates.[13–15] The set of configurations associated with each local minimum on the PEL are named inherent structures (ISs). Each IS has an associated basin, which corresponds to the set of points in configuration space that lead to the same IS when following a steepest-descent path.

A molecular dynamics trajectory can be visualized as an exploration of the PEL, where the system is moving erratically from one basin to the next.[16,17] At low temperatures (T), the system spends a significant fraction of time in the same basin before moving into an adjacent basin. The sequence of anharmonic vibrations around an IS, and the diffusional process of changing IS, controls the system dynamics. Building on Goldstein's intuition, Stillinger developed a thermodynamic formalism based on the total number of ISs, their corresponding energies, and a geometric representation for the shape of each basin.[13,18] This formalism has illuminated the connections between these quantities and the entropic crisis expected to take place close to the ideal glass transition.[15,19]

Only with the availability of significant computational resources has the PEL formalism[13] become a practical tool for shedding light on several important features of the liquid state.[20–26] The onset of two-step relaxation features in structural correlation functions has been shown to correlate[20] with the temperature at which the system begins to explore deeper and deeper ISs. The crossover from mode-coupling dynamics[25] to activated dynamics has been correlated with the temperature at which saddle points are rarely explored,[22,23] the out-of-equilibrium glass state has been associated with the confinement of a system to a single PEL basin,[13] and aging has been described as the progressive exploration of deeper and

18 March 2024 09:23:37

deeper ISs in the attempt to reach the equilibrium IS.[24] The PEL has also been exploited to clarify the concept of an effective temperature for a glass[27,28] and to evaluate the Kauzmann temperature.[29]

The thermodynamic PEL formalism provides an informative expression for the free-energy, in which the configurational degree of freedom is separated from the vibrational component. In the case of anomalous liquids, such as water, the formalism thus offers a powerful method for revealing which statistical properties of the landscape are behind the most common thermodynamic anomalies, such as the density maximum, the compressibility extrema, and the possible existence of a liquid–liquid phase transition (LLPT).[30] For the case of classical molecular models (SPC/E[31] and TIP4P/2005[32]), the landscape approach has consistently predicted the existence of a LLPT at low T and high P.[30,33]

In this article, we quantify the statistical properties of the PEL for the monoatomic ML-BOP model within the Gaussian landscape framework[34,35] for the purpose of computing the system free energy. The equation of state calculated analytically via the volume derivative of the Gaussian landscape model compares very well with the equation of state determined numerically via molecular dynamics simulations, therefore validating the applicability of this PEL approach to the ML-BOP model. Extrapolation of the free energy to low temperatures allows us to detect the presence of a liquid–liquid critical point (LLCP), at $T = 181.5 \pm 1$ K and $P = 1750 \pm 100$ bars, just below the homogeneous nucleation temperature.[7,9] Our calculations are consistent with recent unpublished predictions for the ML-BOP model ($T = 181 \pm 3$ K and $P = 1700 \pm 100$ bars) which are based—to defeat nucleation—on the analysis of density fluctuations in systems with a very small number of water molecules (less than 200).[9] The PEL characterization of this model will make it possible in the near future to tackle important questions on the nature of the amorphous phases of water, including the recently shear-produced (by ball-milling) medium-density amorphous ice.[36]

II. COMPUTATIONAL DETAILS

We have numerically studied a system of $N = 2000$ water molecules interacting via the ML-BOP by performing a series of molecular dynamics simulations in the NVT ensemble using Large-scale Atomic/Molecular Massively Parallel Simulator (LAMMPS) (version 2 Aug 2023).[37] The simulations were performed for a large range of state points, covering densities between $\rho = 0.9$ g/cm^3 and $\rho = 1.5$ g/cm^3 and temperatures between $T = 170$ K and $T = 270$ K. Each simulation was first equilibrated until the potential energy fluctuated around a constant value and for at least 1 ns. Following equilibration, the simulation was continued for 4 ns to generate an equilibrium trajectory. Figure 1 graphically shows the resulting phase (crystalline or liquid) at the end of the simulation for a subset of the studied state points. For the runs that ended in a liquid state, 100 configurations equally spaced in time were minimized using the conjugate gradient method with a stopping tolerance of 10^{-6} kcal/mol. We have then numerically calculated the dynamical matrix for all ISs using the PHONON package of LAMMPS,[37] which we diagonalized to compute the eigenvalues (ω_i^2) associated with each of the $3N - 3$ harmonic modes.

To compute free energies for the ML-BOP system, we have also performed additional NVT simulations starting from a very low density where the system behaves like an ideal gas up to
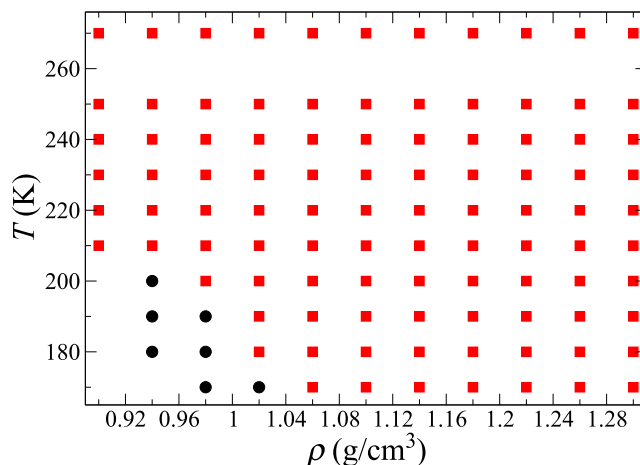

FIG. 1. Graphic representation of the resulting phases for a subset of the studied state points. Red squares indicate the points that did not crystallize during the simulations. Black circles indicate the state points that crystallized (as identified by a sudden drop of the potential energy with time) either during equilibration or during the following production run. The boundary between the two sets of data provides an estimate of the homogeneous nucleation line in the temperature–density plane for the ML-BOP model.

$\rho = 1.14$ g/cm^3 along the $T = 1000$ K isotherm (to avoid crossing the gas–liquid coexistence). We then determine the value of the free energy by thermodynamic integration,[38,39] using the ideal gas as the reference system (see the supplementary material). Further simulations and subsequent thermodynamic integration along the $\rho = 1.14$ g/cm^3 isochore provides the Helmholtz free energy (F) and entropy (S) at $T = 270$ K and $\rho = 1.14$ g/cm^3: $\beta F/N = \beta f = -12.262$ and $S/(Nk_B) = -3.795$ [where $\beta = 1/(k_B T)$ and k_B is the Boltzmann constant]. These values for the free energy and entropy were then used as the starting point for any further thermodynamic cycle.

III. THE GAUSSIAN PEL APPROACH

Several detailed descriptions of the PEL framework introduced by Stillinger and Weber[18,35,40] have been published, including for quantum liquids.[41] Hence, we will limit our discussion here to only the necessary equations and refer the interested reader to the review article[35] and recent investigation of the PEL for TIP4P/2005.[33] Often, it is possible to model the distribution of IS energies (E_{IS}) at a given volume (V) as a Gaussian distribution.[35,42] In this Gaussian landscape model, the distribution of $E_{IS} = Ne_{IS}$ depends on three parameters: (i) the total number of basins $e^{\alpha N}$, which sets the amplitude of the distribution, (ii) the most probable IS energy $E_0 = Ne_0$, which sets the center of the distribution, and (iii) the variance $\Sigma^2 = N\sigma^2$, which sets the width of the distribution. Here (and in the following), the uppercase letters indicate the total system properties, while the lowercase letters (as in e_{IS} and σ^2) indicate the per-particle quantities. For a system of N molecules, the number of basins $\Omega(e_{IS})de_{IS}$ with IS energy per particle between e_{IS} and $e_{IS} + de_{IS}$ is then written as

$$\Omega(e_{IS})\, de_{IS} = \frac{e^{\alpha N}}{\sqrt{2\pi\sigma^2/N}} e^{-N\frac{(e_{IS}-e_0)^2}{2\sigma^2}}\, de_{IS}. \qquad (1)$$

We can then define a configurational entropy for the system as $S_{conf}(T) = k_B \ln \Omega(\langle e_{IS} \rangle_T)$, where $\langle e_{IS} \rangle_T$ is the average IS energy at a temperature of T. For each IS, we can also define a vibrational free energy per particle f_{vib}, which measures how its associated basin is explored at a given temperature T. As a result, the total Helmholtz free energy per particle within the Gaussian landscape model is the sum of three terms,

$$f(T) = \langle e_{IS} \rangle_T + f_{vib}(\langle e_{IS} \rangle_T, T) - TS_{conf}(T)/N. \qquad (2)$$

Once the e_{IS} dependence of the vibrational free energy is provided, the Gaussian landscape model can be solved analytically. The comparison between the theoretical predictions and the numerical simulations provides a way to simultaneously validate the model and estimate the landscape parameters.[35]

IV. RESULTS

We start by determining $\langle e_{IS} \rangle$ as a function of density for each temperature considered, as shown in Fig. 2. A significant T dependence is observed at low densities, where deeper and deeper minima are explored on cooling. At $T = 270$ K, $\langle e_{IS} \rangle$ vs ρ shows a clear double well shape (see the inset of Fig. 2). The region of negative curvature in $\langle e_{IS}(\rho) \rangle$ between $\rho = 0.9$ g/cm^3 and $\rho = 1.3$ g/cm^3 is indicative of the onset of a thermodynamic instability upon cooling. The significance of a region of negative curvature in the density dependence of the potential energy (which, as shown here, arises in the inherent structures) is discussed in Refs. 43 and 44.

Next, we evaluate the vibrational free-energy in the harmonic approximation. First, we determine the vibrational density of states (VDOS) by diagonalizing the dynamical matrices for the IS configurations at each T and ρ considered. From the VDOS, the harmonic vibrational free-energy per particle f_{harm} can be estimated by summing all $3N - 3$ normal modes ω_i as

$$\beta f_{harm} = \frac{1}{N} \sum_{i=1}^{3N-3} \ln \beta \hbar \omega_i,$$
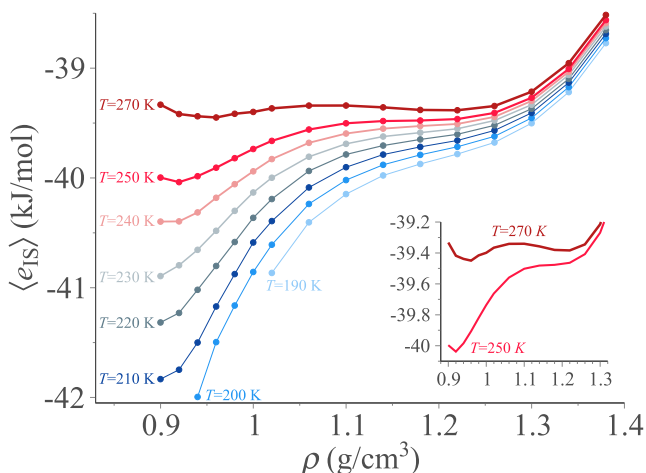

FIG. 2. Density dependence of the inherent structure energies sampled in the liquid state. The inset shows that two clear density basins are present at $T = 270$ K, separated by an energy barrier.
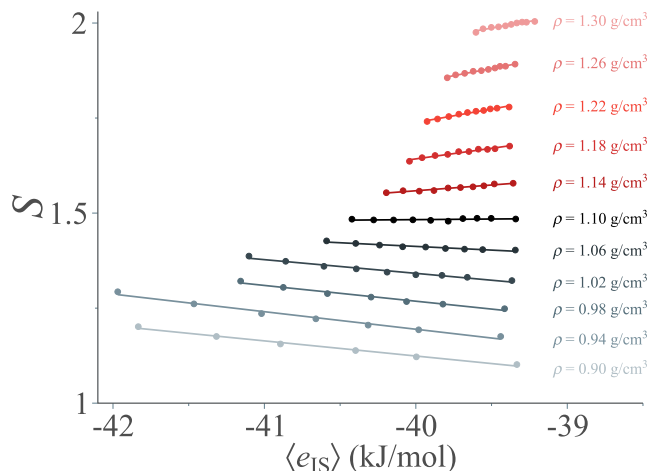

FIG. 3. Shape function $\mathcal{S}$ vs average inherent structure energy $\langle e_{IS} \rangle$ for several studied densities. Lines through the data are the linear fit from which the a and b parameters in Eq. (3) are calculated.

where $\hbar$ is the Planck constant divided by 2π and the e_{IS} dependence is provided by ω_i. To explicitly highlight the dependence of the harmonic free-energy on e_{IS}, we can separate βf_{harm} into a T dependent and an e_{IS} dependent contribution as

$$\beta f_{harm} = 3 \ln \beta A_0 + \frac{1}{N} \sum_{i=1}^{3N-3} \ln \hbar \omega_i / A_0,$$

where A_0 is a constant with the unit of energy that makes both arguments in the log function adimensional (where we have neglected the $3/N$ contribution to the prefactor of the first log function). The last sum depends on the curvature (or shape) of the sampled basin and is usually indicated by the symbol $\mathcal{S}$. Calculating $\mathcal{S}$ vs $\langle e_{IS} \rangle$ provides a complete characterization of the basin free-energy under the harmonic approximation. As performed in previous studies[45] (and supported by the numerical results, see Fig. 3), we assume a linear dependence of $\mathcal{S}$ on $\langle e_{IS} \rangle$ (at a constant volume),

$$\mathcal{S} = a + b\langle e_{IS} \rangle, \qquad (3)$$

where a and b can be determined from a linear fit.

To compute f_{vib}, we assume that the anharmonic contribution to the vibrational free energy per particle f_{anharm} does not depend on e_{IS} but only on T and V[35] and so

$$\beta f_{vib} = 3 \ln \beta A_0 + \mathcal{S} + f_{anharm}(T). \qquad (4)$$

The assumption that the anharmonic correction is independent of e_{IS} could break down in the vicinity of a critical point due to the presence of soft modes. In the case of the liquid–liquid phase transition, the critical point is located at low temperatures where the anharmonic contribution to the basin free energy is less relevant, and, so, this should not be an issue here.

With the expression in Eq. (4) for the vibrational free energy, the Gaussian landscape model can be analytically solved and the temperature dependence of $\langle e_{IS} \rangle$ is predicted to be linear in $(k_B T)^{-1}$,[35]
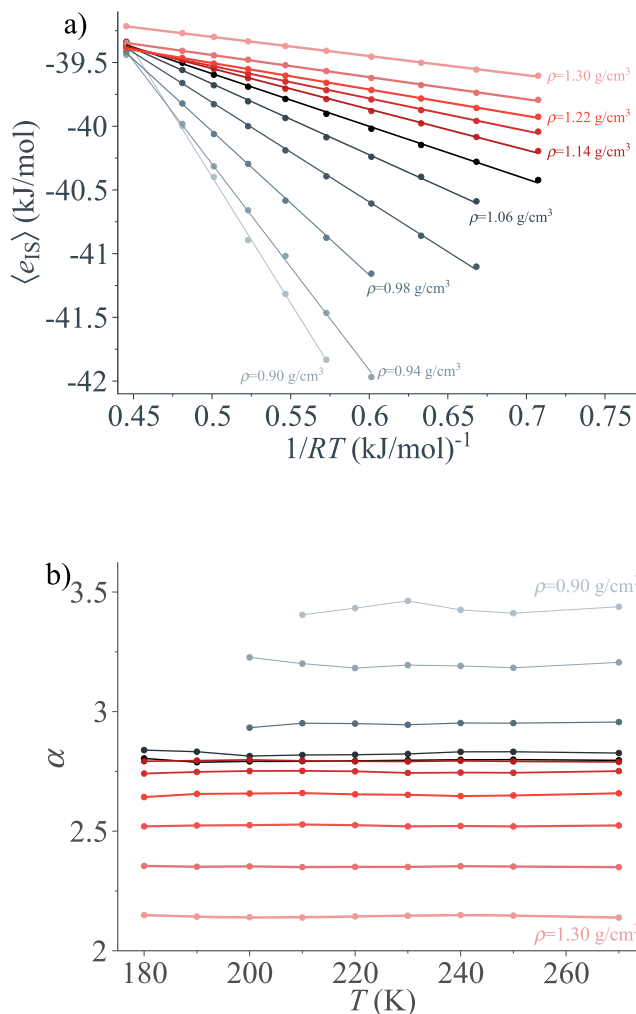
FIG. 4. Evidence in favor of a Gaussian landscape for the ML-BOP model. (a) Plot of the average inherent structure energy $\langle e_{IS} \rangle$ sampled at temperature T as a function of inverse temperature to highlight the linear relationship (here R is the gas constant). (b) Evaluation of the exponent α that determines the total number of states (per particle) as predicted by the Gaussian PEL formalism in Eq. (6). Note that, as predicted, α does not depend on T.

$$\langle e_{IS} \rangle = e_0 - b\sigma^2 - \frac{\sigma^2}{k_B T}. \tag{5}$$

Figure 4(a) confirms that this prediction is extremely well verified for the ML-BOP at all investigated temperatures. A linear fit of $\langle e_{IS} \rangle$ vs $(k_B T)^{-1}$ at each density provides both σ^2 and $e_0 + b\sigma^2$ [and thus e_0 since we already know b from Eq. (3)].

Another test for the Gaussianity of the PEL for the ML-BOP model is provided by the configurational entropy. From a thermodynamic point of view, $S_{conf}(T)$ can be evaluated by subtracting the vibrational entropy from the liquid entropy[21,29,35,46,47] (see the supplementary material for more details). The results of these calculations, including anharmonic corrections, are reported in Fig. 5.
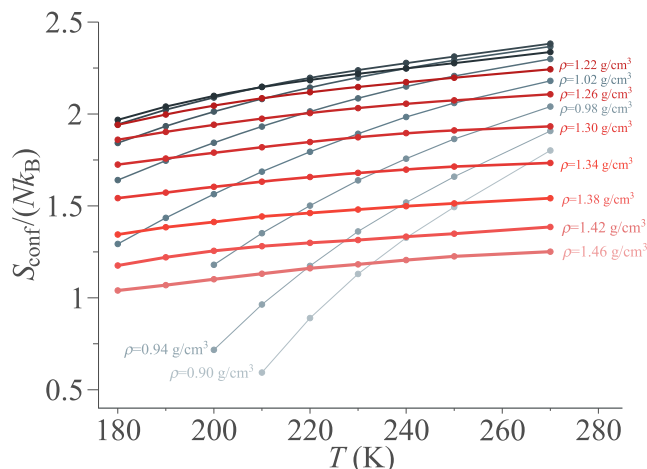

FIG. 5. Configurational entropy (S_{conf}) evaluated via thermodynamic integration for different isochores.

From the Gaussian PEL point of view, $S_{conf}(T)$ (in the thermodynamic limit) can be obtained from Eq. (1) as

$$S_{conf}(T)/(Nk_B) = \alpha - \frac{(\langle e_{IS} \rangle_T - e_0)^2}{2\sigma^2}. \tag{6}$$

A plot of $S_{conf}(T)/(Nk_B) + (\langle e_{IS} \rangle_T - e_0)^2/(2\sigma^2)$ as a function of T for each density should, therefore, be constant and provide the value of the landscape parameter α. Such a plot is shown in Fig. 4(b), which again provides strong support for the validity of the Gaussian description of the PEL for the ML-BOP model. The density dependence of all PEL parameters (a, b, e_0, σ^2, and α) is shown in Fig. 6. However, we note that while the Gaussian landscape framework properly models the ML-BOP system at the studied T and ρ, any extrapolation significantly outside the investigated region (for example when $S_{conf} \approx 0$) should be taken with care.

V. PEL-EOS

In the PEL approach, the equation of state (EOS) $P(V,T)$ can be expressed as a power series of the temperature (T^i). In the harmonic approximation for the vibrational free energy, i is limited to the interval -1 to $+1$. The coefficients of the T^i terms have well defined expressions, which we recall here as follows:[35,48]

$$\mathcal{P}_{T^{-1}}(V) = \frac{N}{2k_B} \frac{d}{dV}\sigma^2, \tag{7}$$

$$\mathcal{P}_{T^0}(V) = -N\frac{d}{dV}(e_0 - b\sigma^2), \tag{8}$$

$$\mathcal{P}_{T^1}(V) = Nk_B \frac{d}{dV}\left(\alpha - a - be_0 + \frac{b^2\sigma^2}{2}\right). \tag{9}$$

If anharmonic contributions to the free energy are considered (as they are here), then additional powers of T^i (up to $T^{i_{max}}$) are required (we discuss the details of including these anharmonic contributions
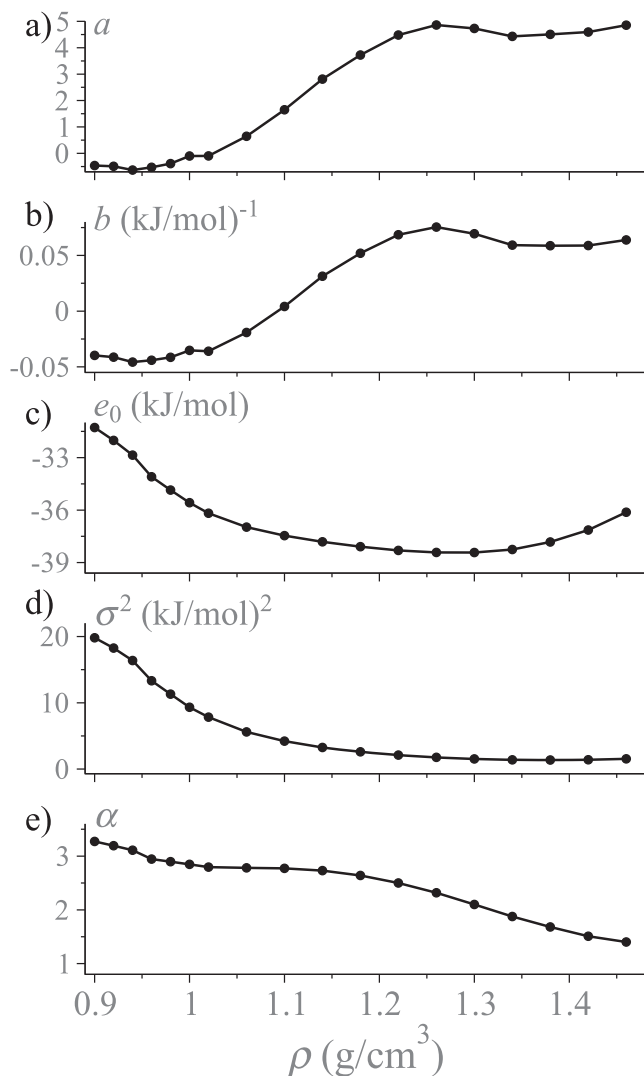
FIG. 6. Density dependence of the parameters defining the Gaussian landscape for the ML-BOP model. Panels (a) and (b) report the coefficients defining the harmonic shape of the PEL basins [Eq. (3)]. Panels (c)–(e) report the parameters of the Gaussian distribution of basins [Eq. (1)].

Figure 7 compares the ML-BOP PEL-EOS, as determined by Eq. (10) (i.e., with the additional contributions from the anharmonic free energy as discussed in the supplementary material), with the "exact" molecular dynamics results at two different temperatures. The agreement is remarkable providing a further (and final) test for the applicability of the Gaussian landscape approach here.

Using the Gaussian landscape framework, we can also valuate the EOS of the liquid at temperatures below the homogeneous
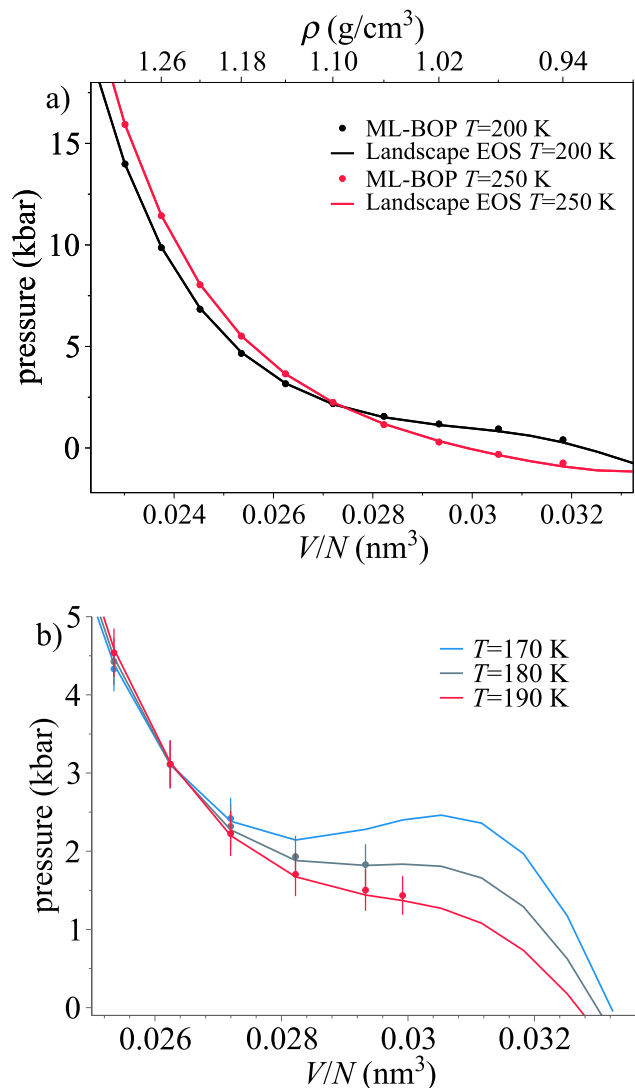
in Sec. S2.2 of the supplementary material).[33] The EOS can then be written as

$$P(V, T) = \sum_{i=-1}^{i_{max}} \mathcal{P}_{T^i}(V) T^i. \tag{10}$$

Note that—since $\mathcal{P}_{T^{-1}}(V)$ involves only the V derivative of σ^2—the low T behavior of the pressure is controlled solely by the slope of σ^2. Since an increase in P upon cooling is a thermodynamic signature of a density anomaly [a minimum in $P(T)$ at constant V is equivalent to a maximum in $\rho(T)$ at constant P by a Maxwell relation]. Thus, density maxima are expected to be found for the ML-BOP model [see Fig. 6(d)].

FIG. 7. (a) Comparison between the equation of state (EOS) calculated via molecular dynamics and the EOS calculated using the landscape expression at two different temperatures. (b) EOS for different temperatures in the region where nucleation takes place, suggesting the presence of an unreachable liquid–liquid critical point. Solid lines are the predicted EOS from the Gaussian landscape framework, and solid circles represent the pressures computed directly via molecular dynamics simulations (error bars represent the standard deviation in the computed averages).

nucleation line (i.e., at temperatures where the liquid is not directly accessible in molecular dynamics simulations). A small extrapolation of the EOS at three close-by low temperatures is shown in Fig. 7(b), with the lowest isotherm displaying a clear van der Waals loop, indicative of a first-order phase transition between two liquid phases (adding one more example to the ever expanding list of classical and quantum-based models for water that do show a liquid–liquid transition[49–56]).

In Fig. 7, we also report the pressures evaluated directly from molecular dynamics simulations for densities where the system does not crystallize. Where the two methods can be compared, quite good agreement is observed. This agreement suggests that the values following a small extrapolation of less than 20 K in the low-density region—which cannot be accessed directly by molecular dynamics—are trustworthy.

From the PEL-EOS, the low temperature phase diagram can be calculated, including the temperature of maximum density (TMD) line, the compressibility maxima line, the liquid–liquid coexistence line, and the ideal glass line. To determine the ideal glass line (the temperature at which $S_{conf} = 0$) within the Gaussian landscape framework, we calculate the Kauzmann temperature as[35]

$$k_B T_K = \left(\sqrt{\frac{2\alpha}{\sigma^2}} - b \right)^{-1}. \quad (11)$$

At T_K, $\langle e_{IS} \rangle_T$ reaches the value

$$\langle e_{IS} \rangle_{T_K} = e_0 - \sqrt{2\alpha}\sigma. \quad (12)$$

All lines are shown in Fig. 8 in both the T–P and ρ–T planes, for $T \geq 171$ K. This figure shows that, within the Gaussian landscape approximation, the Kauzmann line in the low-density liquid region encounters the coexistence line at $T \approx 171$ K. Below T_K, the system is in an ideal glass state and the configurational entropy has vanished. The high density liquid now coexists with a (low-density) glass and not with a liquid anymore. This means that the evaluation of a proper phase–coexistence boundary requires the inclusion of further approximations, specifically on how to model the free-energy of a glass.

We note that the estimated low density liquid T_K is significantly higher than the experimentally detected water calorimetric glass transition,[57,58] possibly an effect of the crossover from the Gaussian landscape to a different functional form, which could take place in the ML-BOP no-man's land. Indeed, in models of network forming liquids, the ground state may retain a finite entropy due to the number of distinct configurations with different ring statistics and hence different topologies (see, for example, Refs. 59–61 for primitive models and Refs. 62 and 63 for silica). In these models, the Kauzmann temperature has been found to be 0 K.

The Kauzmann temperature for the high density liquid is located at temperatures below $T = 100$ K. Despite requiring a significant extrapolation from the temperatures considered in the molecular dynamics simulations, the location of this line is consistent with the much larger diffusivity of the high density liquid as compared to the low density liquid (we show the Kauzmann temperature line for both liquids in Fig. S7 of the supplementary material).
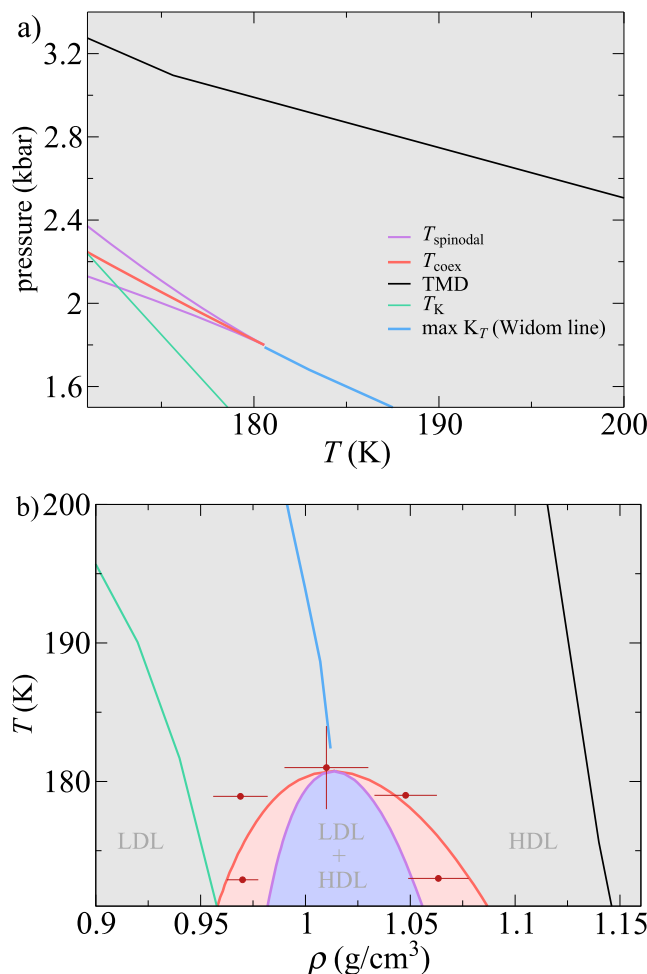

FIG. 8. Potential energy landscape (PEL) phase diagram of the ML-BOP model in the (a) pressure–temperature (P–T) plane and (b) density–temperature (ρ–T) plane. The liquid–liquid critical point (LLCP) is located at $T = 181.5$ K and $P = 1750$ bars. The phase diagrams are shown down to a temperature of $T = 171$ K, which is where the Kauzmann temperature line (T_K) meets the coexistence line. The red data points in panel (b) correspond to the liquid–liquid coexistence points computed in Ref. 9.

VI. CONCLUSIONS

In this article, we have applied the potential energy landscape (PEL) formalism to a recently proposed model for water (ML-BOP) based on a machine learning optimization of the Tersoff potential.[1] This monoatomic model for water generates the tetrahedral geometry via a three-body contribution to the interaction potential, similar to the mW model.[5] The short-range nature of the potential (which does not explicitly account for charge–charge interactions) makes it possible to simulate large systems for long times, even with limited computational resources, while still properly reproducing the thermodynamic behavior of the real system.

We have demonstrated that the PEL of ML-BOP can be accurately modeled by a Gaussian distribution of inherent structure energies per particle (e_{IS}). The Gaussian landscape model predicts

that the T-dependence of e_{IS} follows an inverse T law [Eq. (5)] and that the configurational entropy (defined as the difference between the liquid entropy and the vibrational entropy of the sampled basins) goes with $(e_{IS}(T) - e_0)^2$. Both predictions are remarkably satisfied by ML-BOP [Figs. 4(a) and 4(b)] at all studied densities, thereby validating the Gaussianity of the PEL and providing an accurate numerical estimate of the PEL parameters from which the EOS can be determined.

The resulting equation of state (EOS) perfectly reproduces the thermodynamic properties of the model in the region where it can be simulated, but, more importantly it offers a sound functional form to extrapolate within the Gaussian landscape hypothesis the phase behavior of the system at temperatures lower than those numerically accessible (due to the onset of crystallization). A quite small extrapolation demonstrates that the model free-energy surface is characterized by two distinct phases, separated by a first order transition line, i.e., between two liquids with different densities. The liquid–liquid critical point (LLCP) is located in the region where crystal nucleation prevents the direct observation of the critical point for the system size considered in this article. Since basins associated with crystalline configurations are not included in the PEL formalism, the resulting EOS is not influenced by the presence of crystals, making it possible to demonstrate that a LLCP exists in the model, even if it cannot be reached. This makes the ML-BOP unique in the context of all previously studied models of water displaying a LLCP since it offers the possibility to investigate how the presence of the LLCP influences the kinetics of nucleation. This is different from models where hydrogen atoms are explicitly taken into account (TIP4P/2005, TIP4P/Ice, and MB-pol) as crystallization has never been reported in these models within the presently investigated μs scale. From a semantic point of view, one could prefer to say that when (either in simulations or in experiments) nucleation prevents the approach to the critical point (as in the present case), the critical point does not exist in practice, and, so, it is unproductive to discuss the presence of a LLCP (regardless of whether it exists or not). However, by using the PEL formalism, we have clearly shown that the disordered free-energy surface of the ML-BOP model does, indeed, possess a LLCP and its presence influences the shape of the surface.

Importantly, we have also shown that the influence of the LLCP extends to supercooled liquid states where the structural relaxation time is shorter than the nucleation time. We use the word "influence" to stress that the presence of a critical point fixes the functional form of the free energy and, as a result, the functional form of the equation of state. Close to the critical point and above the nucleation line (where the liquid has the time to equilibrate properly before nucleation takes place), the behavior of the density and energy fluctuations is still related to the presence of the nearby thermodynamic phase transition.

It is also interesting to observe that the decrease in the configuration entropy [the log of the number of existing inherent structures (ISs) with energy $\langle e_{IS}\rangle_T$] on cooling is quite fast, especially at low densities. Indeed, the estimated Kauzmann temperature at ambient pressure is 190 K, only 10–20 K below the homogeneous nucleation temperature. In the ML-BOP model, crystal formation resolves the Kauzmann paradox.[19]

Finally, we stress that the PEL builds upon a description of each liquid configuration as composed of an IS supplemented by a vibrational distortion. Then, in the PEL approach, a generic glass is nothing more than an IS sampled with a low T-vibrational component that does not allow for exploring nearby PEL basins. In this respect, each IS is a potential glass of the system, highlighting the continuity of amorphous ices spanning the entire density range where a liquid state exists. Among all glasses, a particular theoretical relevance is played by the Kauzmann glasses, defined as the ISs of lowest energy (i.e., the ones for which the configurational entropy vanishes). Ultrastable glasses, obtained by vapor deposition[64] and/or by artificial computational paths via swap dynamics,[65,66] polymerization,[67] and local density homogenization,[68] are examples of glasses with quite low e_{IS}. The ability of the PEL formalism to separate configurational properties from those that are vibrational in nature has been exploited to build an out-of-equilibrium free-energy expression valid for all cases in which the out-of-equilibrium state can be considered as one of the glasses sampled in thermal equilibrium (same IS and same basin shape).[27,69] We, therefore, foresee an application of the PEL formalism to shear-induced glass formation, including the recently reported ball-milling intermediate ice.[36]

SUPPLEMENTARY MATERIAL

The supplementary material discusses, in more depth, the Gaussian landscape model, the calculation of the reference free energy, the liquid and crystal vibrational density of states, and the Kauzmann line for the two liquids.

ACKNOWLEDGMENTS

AUTHOR DECLARATIONS

Conflict of Interest

The authors have no conflicts to disclose.

Author Contributions

Andreas Neophytou: Conceptualization (equal); Data curation (equal); Writing – original draft (equal); Writing – review & editing (equal). **Francesco Sciortino**: Conceptualization (equal); Data curation (equal); Funding acquisition (lead); Writing – original draft (equal); Writing – review & editing (equal).

DATA AVAILABILITY

The data that support the findings of this study are available within the article. The public domain LAMMPS code has been used to generate trajectories for all different temperatures and densities as well as the inherent structures and the associated Hessian.

18 March 2024 09:23:37

REFERENCES

[1] H. Chan, M. J. Cherukara, B. Narayanan, T. D. Loeffler, C. Benmore, S. K. Gray, and S. K. Sankaranarayanan, Nat. Commun. **10**, 379 (2019).

[2] J. Behler, J. Chem. Phys. **145**, 219901 (2016).

[3] V. L. Deringer, M. A. Caro, and G. Csányi, Adv. Mater. **31**, 1902765 (2019).

[4] T. Mueller, A. Hernandez, and C. Wang, J. Chem. Phys. **152**, 050902 (2020).

[5] V. Molinero and E. B. Moore, J. Phys. Chem. B **113**, 4008 (2009).

[6] E. B. Moore and V. Molinero, Nature **479**, 506 (2011).

[7] D. Dhabal, S. K. Sankaranarayanan, and V. Molinero, J. Phys. Chem. B **126**, 9881 (2022).

[8] D. Dhabal and V. Molinero, J. Phys. Chem. B **127**, 2847 (2023).

[9] D. Dhabal, R. Kumar, and V. Molinero, chemRxiv:10.26434 (2023).

[10] P. A. Taylor and M. J. Stevens, Eur. Phys. J. E **46**, 97 (2023).

[11] V. K. Sinha, A. K. Metya, and C. K. Das, Fluid Phase Equilib. **577**, 113985 (2024).

[12] M. Goldstein, J. Chem. Phys. **51**, 3728 (1969).

[13] F. H. Stillinger, *Energy Landscapes, Inherent Structures, and Condensed-Matter Phenomena* (Princeton University Press, 2015).

[14] D. Wales, *Energy Landscapes: Applications to Clusters, Biomolecules and Glasses, Cambridge Molecular Science* (Cambridge University Press, 2004).

[15] P. G. Debenedetti and F. H. Stillinger, Nature **410**, 259 (2001).

[16] A. Heuer, J. Phys.: Condens. Matter **20**, 373101 (2008).

[17] B. Doliwa and A. Heuer, Phys. Rev. Lett. **91**, 235501 (2003).

[18] F. H. Stillinger and T. A. Weber, Phys. Rev. A **25**, 978 (1982).

[19] W. Kauzmann, Chem. Rev. **43**, 219 (1948).

[20] S. Sastry, P. G. Debenedetti, and F. H. Stillinger, Nature **393**, 554 (1998).

[21] S. Sastry, Nature **409**, 164 (2001).

[22] L. Angelani, R. Di Leonardo, G. Ruocco, A. Scala, and F. Sciortino, Phys. Rev. Lett. **85**, 5356 (2000).

[23] K. Broderix, K. K. Bhattacharya, A. Cavagna, A. Zippelius, and I. Giardina, Phys. Rev. Lett. **85**, 5360 (2000).

[24] W. Kob, F. Sciortino, and P. Tartaglia, Europhys. Lett. **49**, 590 (2000).

[25] W. Götze, *Complex Dynamics of Glass-Forming Liquids: A Mode-Coupling Theory* (Oxford University Press, 2009), Vol. 143.

[26] Y. Chen, D. Campi, M. Bernasconi, and R. Mazzarello, Adv. Funct. Mater. (published online).

[27] F. Sciortino and P. Tartaglia, Phys. Rev. Lett. **86**, 107 (2001).

[28] S. Mossa and F. Sciortino, Phys. Rev. Lett. **92**, 045504 (2004).

[29] F. Sciortino, W. Kob, and P. Tartaglia, Phys. Rev. Lett. **83**, 3214 (1999).

[30] F. Sciortino, E. La Nave, and P. Tartaglia, Phys. Rev. Lett. **91**, 155701 (2003).

[31] H. J. C. Berendsen, J. R. Grigera, and T. P. Straatsma, J. Phys. Chem. **91**, 6269 (1987).

[32] J. L. Abascal and C. Vega, J. Chem. Phys. **133**, 234502 (2010).

[33] P. H. Handle and F. Sciortino, J. Chem. Phys. **148**, 134505 (2018).

[34] B. Derrida, Phys. Rev. B **24**, 2613 (1981).

[35] F. Sciortino, J. Stat. Mech.: Theory Exp. **2005**, P05015.

[36] A. Rosu-Finsen, M. B. Davies, A. Amon, H. Wu, A. Sella, A. Michaelides, and C. G. Salzmann, Science **379**, 474 (2023).

[37] A. P. Thompson, H. M. Aktulga, R. Berger, D. S. Bolintineanu, W. M. Brown, P. S. Crozier, P. J. in't Veld, A. Kohlmeyer, S. G. Moore, T. D. Nguyen *et al.*, Comput. Phys. Commun. **271**, 108171 (2022).

[38] D. Frenkel and B. Smit, *Understanding Molecular Simulation: From Algorithms to Applications* (Elsevier, 2023).

[39] C. Vega, E. Sanz, J. Abascal, and E. Noya, J. Phys.: Condens. Matter **20**, 153101 (2008).

[40] F. H. Stillinger and P. G. Debenedetti, J. Chem. Phys. **116**, 3353 (2002).

[41] N. Giovambattista and G. E. Lopez, Phys. Rev. Res. **2**, 043441 (2020).

[42] A. Heuer and S. Büchner, J. Phys.: Condens. Matter **12**, 6535 (2000).

[43] F. Sciortino, P. H. Poole, U. Essmann, and H. Stanley, Phys. Rev. E **55**, 727 (1997).

[44] J. Russo, F. Leoni, F. Martelli, and F. Sciortino, Rep. Prog. Phys. **85**, 016601 (2022).

[45] N. Giovambattista, F. W. Starr, and P. H. Poole, J. Chem. Phys. **147**, 044501 (2017).

[46] B. Coluzzi, G. Parisi, and P. Verrocchio, J. Chem. Phys. **112**, 2933 (2000).

[47] L. Berthier, M. Ozawa, and C. Scalliet, J. Chem. Phys. **150**, 160902 (2019).

[48] E. La Nave, S. Mossa, and F. Sciortino, Phys. Rev. Lett. **88**, 225701 (2002).

[49] P. H. Poole, F. Sciortino, U. Essmann, and H. Stanley, Nature **360**, 324 (1992).

[50] P. G. Debenedetti, F. Sciortino, and G. H. Zerze, Science **369**, 289 (2020).

[51] J. Weis, F. Sciortino, A. Z. Panagiotopoulos, and P. G. Debenedetti, J. Chem. Phys. **157**, 024502 (2022).

[52] T. E. Gartner III, P. M. Piaggi, R. Car, A. Z. Panagiotopoulos, and P. G. Debenedetti, Phys. Rev. Lett. **129**, 255702 (2022).

[53] A. Eltareb, G. E. Lopez, and N. Giovambattista, Sci. Rep. **12**, 6004 (2022).

[54] Y. Li, J. Li, and F. Wang, Proc. Natl. Acad. Sci. U. S. A. **110**, 12209 (2013).

[55] Y. Ni and J. Skinner, J. Chem. Phys. **144**, 214501 (2016).

[56] J. C. Palmer, P. H. Poole, F. Sciortino, and P. G. Debenedetti, Chem. Rev. **118**, 9129 (2018).

[57] G. Johari, A. Hallbrucker, and E. Mayer, Nature **330**, 552 (1987).

[58] K. Amann-Winkel, C. Gainaru, P. H. Handle, M. Seidl, H. Nelson, R. Böhmer, and T. Loerting, Proc. Natl. Acad. Sci. U. S. A. **110**, 17720 (2013).

[59] A. Moreno, S. Buldyrev, E. La Nave, I. Saika-Voivod, F. Sciortino, P. Tartaglia, and E. Zaccarelli, Phys. Rev. Lett. **95**, 157802 (2005).

[60] A. Moreno, I. Saika-Voivod, E. Zaccarelli, E. La Nave, S. Buldyrev, P. Tartaglia, and F. Sciortino, J. Chem. Phys. **124**, 204509 (2006).

[61] F. Smallenburg and F. Sciortino, Nat. Phys. **9**, 554 (2013).

[62] I. Saika-Voivod, P. H. Poole, and F. Sciortino, Nature **412**, 514 (2001).

[63] A. Saksaengwijit, J. Reinisch, and A. Heuer, Phys. Rev. Lett. **93**, 235701 (2004).

[64] S. Singh, M. D. Ediger, and J. J. De Pablo, Nat. Mater. **12**, 139 (2013).

[65] L. Berthier and D. R. Reichman, Nat. Rev. Phys. **5**, 102 (2023).

[66] C. Scalliet, B. Guiselin, and L. Berthier, Phys. Rev. X **12**, 041028 (2022).

[67] M. Ozawa, Y. Iwashita, W. Kob, and F. Zamponi, Nat. Commun. **14**, 113 (2023).

[68] T. Yanagishima, J. Russo, R. P. Dullens, and H. Tanaka, Phys. Rev. Lett. **127**, 215501 (2021).

[69] S. Mossa, E. La Nave, F. Sciortino, and P. Tartaglia, Eur. Phys. J. B **30**, 351 (2002).